# On the interpretation of gravity tide residuals in the Iberian Peninsula

José Fernández, Manel Fernández, Luis Miguelsanz, Antonio G. Camacho

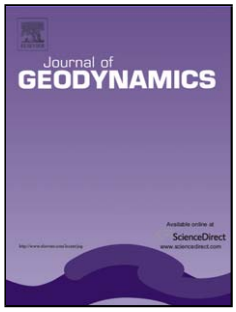


Title: On the interpretation of gravity tide residuals in the Iberian Peninsula

Authors: José Fernández, Manel Fernández, Luis Miguelsanz, Antonio G. Camacho

PII: S0264-3707(07)00032-4
DOI: doi:10.1016/j.jog.2007.03.006
Reference: GEOD 813

To appear in: *Journal of Geodynamics*

Received date: 12-6-2006
Revised date: 2-3-2007
Accepted date: 12-3-2007

Please cite this article as: Fernández, J., Fernández, M., Miguelsanz, L., Camacho, A.G., On the interpretation of gravity tide residuals in the Iberian Peninsula, *Journal of Geodynamics* (2007), doi:10.1016/j.jog.2007.03.006

# ON THE INTERPRETATION OF GRAVITY TIDE RESIDUALS IN THE IBERIAN PENINSULA

**José Fernández[(1),(*)], Manel Fernández[(2)], Luis Miguelsanz[(1)], Antonio G. Camacho[(1)]**

[(1)]Instituto de Astronomía y Geodesia (CSIC-UCM). Fac. C. Matemáticas. Ciudad Universitaria, Plaza de Ciencias, 3. 28040-Madrid, Spain.

Tel: +34 91 394 46 32, Fax: +34 91 394 46 15, email: jose_fernandez@mat.ucm.es

[(2)]Group of Dynamics of the Lithosphere (GDL), Department of Structure and Dynamics of the Earth, Institute of Earth Sciences, CSIC. Sole Sabaris s/n. Barcelona 08028. Spain.

Tel: +34 93 409 54 10, Fax: +34 93 411 00 12, email: mfernandez@ija.csic.es

(*) Corresponding author

**Abstract.**

The interpretation of tidal gravity final residuals is an issue of high debate in geodesy. Whereas some authors suggest that final residuals are related to possible instrumental and measurement errors or to errors in the evaluation of the oceanic load computations, others propose certain empirical relationships between the gravity tidal residuals and the heat flow or the tectonothermal age of the lithosphere which, in turn, reveal structural variations with respect to a homogeneous elastic model. We examine such relationships in the Iberian Peninsula by studying correlations between the cosine component of the final residual vector for the $M_2$ and $O_1$ waves of the gravity tide potential and different structural parameters for a total of 21 gravity tide stations. The selected parameters, which are related to the capability of the lithosphere to deform, include surface heat flow as the main parameter and, to a lesser extend, lithospheric strength, Moho temperature and tectonothermal age of the lithosphere. Our study agrees with previous results by other authors and does not demonstrate the existence of empirical relationships between the gravity residuals and structural parameters. Actually, when we consider the most precise observations and recent ocean tide models the final residuals are mostly uncorrelated noise. Our results also agree with theoretical studies proposing that the distortions of the tidal gravity field from spherical symmetry are very small and hardly to observe.

**KEYWORKS:** Tidal gravity residuals - Heat flow – Integrated lithospheric Strength – Moho temperature - Iberian Peninsula

## 1. INTRODUCTION

The observation of gravity tides, which began systematically from the 1960's onwards, now covers a great part of the world's surface (e.g., Melchior, 1994a). The density of information existing in Europe, in particular in Spain, and stored in the data bank of the International Center of Earth Tides (ICET - www.astro.oma.be/ICET/) can be used to make predictions and conduct correlation tests on the tidal residuals.

When evaluating the amplitudes and phase-lags of the harmonic components of the tide potential from observed data and comparing them with those obtained for an Earth model which does not includes either oceans or atmosphere, we find that they differ substantially (Melchior, 1983). This disagreement may mainly have two origins: geodynamics and local characteristics of the crust, or the indirect oceanic effect produced by an inappropriate correction for this effect (J. Fernández et al., 1992).

Using the notation introduced by Melchior (1983), we have the following vectors (amplitude, phase) related to the tide waves, see Figure 1: $\mathbf{R}(R,0)$, is the body tide vector of an elastic Earth model lunisolar potential; $\mathbf{A}(A,\alpha)$ is the observed vector, normally obtained through least squares analysis of gravimetric observations ; $\mathbf{L}(L,\lambda)$ is the computed oceanic loading and attraction vector; $\mathbf{B}(B,\beta) = \mathbf{A} - \mathbf{R}$ is a first residual vector; $\mathbf{X}(X,\chi) = \mathbf{B} - \mathbf{L}$ is the final residual, which must represent the noise of the observations and the discrepancies with the models used (Melchior and Ducarme, 1991). The sine component gives us an indication of the error made in vectors **A**, **R** and **L** (Melchior and De Becker, 1983). The cosine component of this final residual vector reflects the heterogeneity that distinguishes the real Earth from the model considered, although, according to Baker and Bos (2003), calibration errors would also affect the cosine component.

One can expect a certain degree of correlation with parameters such as the crust thickness and age, lithosphere thickness, geoid undulations, volcanic nature of the soil, etc. As a result, during the Eighties and Nineties, different correlation studies were conducted using the final residual vectors of different waves of the harmonic development of the gravity tide potential. Some of the studies (Melchior and Ducarme 1991, Melchior and De Becker 1983, Melchior et al. 1986, Yanshin et al. 1986, Jeligovski et al. 1988, Robinson 1989, Robinson 1991, Robinson 1993) show a correlation

between heat flow values and the component of the gravity tide residual which is in-phase with the body tide (the cosine component) for several waves of the gravity tide potential. The correlation appears more clearly between the cosine component of final residual of the main lunar $M_2$ wave (Jeligovski et al., 1988). Positive and negative anomalies around an average value, in absolute terms, of 1 μGal ($10^{-8}$ m $s^{-2}$) appear associated, respectively, with areas of thin crust, high heat flow values, and recent basaltic-type volcanic activity, and with stable structures that have a deeper Mohorovicic discontinuity and lower heat flow. Robinson (1989, 1991) associates the correlation found in his studies to features in the upper crust, suggesting a measurable upper crustal tidal response.

Contrary to those results, Rydelek et al. (1991) do not find any significant correlation between surface heat flow values and the cosine component of the gravimetric tide wave residual. They impute their results to the level of errors in both observations. J. Fernández et al. (1992) and Arnoso et al. (2001) fail to find this correlation in the results obtained for Lanzarote, an island with an average crustal thickness of 11.5 km, recent basaltic-type volcanic activity, an average heat flow value on the island of 109 mW $m^{-2}$, and anomalous zones with values of up to 130 W $m^{-2}$ (J. Fernández et al., 1992). However, the $M_2$ wave residual was practically zero.

Melchior (1995) describes a new interpretation of the correlation found between the heat flow values and the tide residuals after reviewing and reanalyzing the original tide data of 300 stations (Melchior, 1994a). This review takes into account the objections raised by Rydelek et al. (1991), removing sources of error, essentially the instrument calibration errors. Melchior (1995) proposes a correlation between the tidal gravity residuals and the age of the tectonic provinces as an alternative to correlation with the heat flow: negative residuals in areas older than 800 m.y. (-0.21 ± 0.10 μGal) and positive residuals in areas younger than 250 m.y. (0.36 ± 0.12 μGal).

Shukowsky and Mantovani (1999) performed some statistical tests on the World Gravity Earth Tides data set, trying to explore the possible relationship between Earth tidal gravity and some physical properties of the lithosphere. Autocorrelation analysis showed that $M_2$ tidal gravity residuals are clearly correlated up to a distance of about 500 km. The regression analysis between these $M_2$ residuals and the effective elastic thickness of the lithosphere parameter (EET) shows that both quantities are highly correlated, the correlation line being EET = 69.85 ($\pm$ 2.63) - 15.48 ($\pm$ 3.19)$\Delta g$ ,

with a correlation coefficient R = -0.82. This strong linear dependence creates an alternative for estimating the EET parameter where no large gravity surveys exist, successfully applied to construct continental EET maps for the South American and African plates (Mantovani et al., 2005).

Baker and Bos (2003) used tidal gravity observations from spring gravimeters and superconducting gravimeters from the Global Geodynamics Project (Hinderer and Crossley, 2000) to test several body and ocean tide models. They conclude that the Schwiderski (1980) ocean tide model gives anomalous results in certain places and there are ocean tide models (such as FES 95, FES 99 or TPXO) in a better agreement with the tidal gravity measurements. Gravimetric factors corrected for ocean tide loading and attraction using different ocean tide models can be, in turn, used for testing the body tide models, but the interpretation of the results is subject to discussion due to calibration errors or uncertainties in the ocean tide loading corrections. The estimated calibration errors at the European stations in the paper by Baker and Bos (2003) are of the order of 0.1 per cent, so it is not even possible to distinguish between the DDW (Dehant, Defraigne and Wahr, see Dehant et al., 1999) elastic and inelastic Earth models, whose gravimetric factors differ only by 0.12 per cent. Outside Europe (Baker and Bos, 2003), the corrected gravimetric factors differ from the DDW models by between –0.2 and + 0.3 per cent.

It may be premature to assume that these differences are caused by lateral heterogeneities in the Earth's structure. According to Wang (1991), lateral heterogeneities in the Earth's mantle affect both the in-phase and out-of-phase components, but he calculated a global maximum effect of 0.03 μGal (assuming no amplification from seismic to tidal periods). His model gives effects lesser than 0.01 μGal for Europe. The maximum effect on the gravimetric factors would be of approximately $\pm$ 0.05 per cent, and the effect on the phase shifts would be of a similar magnitude (Wang, 1991). Nevertheless, it is possible that shorter-wavelength lateral changes in Earth structure give larger effects. According to the finite-element model of Zürn et al (1976), a subducting plate may affect the vertical body tide displacement up to a + 0.8 per cent and, therefore, the gravimetric factor could be increased by a few tenths of a per cent (at least, over the leading edge of the subducting plate). Molodenskii and Kramer (1980) developed a theory to investigate the influence of lateral inhomogeneities on gravity tides by means of a spherical harmonic representation of the ocean-

continent distribution of the Earth. They found that the tidal gravimetric factor was affected no more than 0.75% in any of their models. In order to investigate the influence of lateral heterogeneities smaller in horizontal extent, the variations in seismic velocities in North America given by Herrin and Taggart (1962) were used. As a result, a maximum variation of 0.15% for the gravimetric factor was found (throughout the USA). So a large scale spatial fluctuation of heat flow should have a greater influence on tidal gravity than localized fluctuations.

Over the last 30 years, numerous gravimetric tide observations have been made on the Iberian Peninsula at a total of 21 stations distributed as displayed in Figure 2. These results have provided a model for gravimetric tide corrections throughout the area (Camacho and Vieira, 1990). Also available is data regarding surface heat flow and radiogenic heat production in much of the Iberian Peninsula (M. Fernández et al., 1998) and data from several seismic campaigns (vertical incidence and wide angle) with which the internal structure of the crust and its thickness can be determined (Vera, 2004).

In this paper we use a correlation study to examine whether any relationship exists between the cosine component of the final residual vector obtained for certain gravity tide potential waves and different geophysical parameters that are related to the capability of the lithosphere to deform (surface heat flow, lithospheric strength, Moho temperature and tectonothermal age of the lithosphere) considering the 21 stations on the Iberian Peninsula. The study, which includes different ocean tide models, uses the results of the harmonic analysis of the gravity tide stations supplied by the IUGG International Center of Earth Tides (ICET) to ensure comparability of results with previous studies.

## 2. DATA

The Iberian Peninsula has undergone, since the lower Paleozoic, several tectonothermal episodes which gave rise to the presently observed geological units. The western half of Iberia corresponds to the Variscan Iberian Massif, which is the oldest and most stable region of the Iberian Peninsula. The subsequent Mesozoic extensional tectonics was responsible for the opening of the Atlantic and Tethys oceans and the corresponding passive margins which extended into the present-day emerged Peninsula. Later on, the Alpine orogeny resulted in a strong deformation of the northern and southern margins of Iberia. The Pyrenees were built up in the northern margin, whereas incipient subduction

developed in the Cantabrian margin. The Betics and the Balearic Promontory formed along the southern margin. The Ebro and Guadalquivir basins were added as foreland basins to the Pyrenees and the Betics, respectively. The interior of Iberia was also deformed in Alpine times with basement-involved structures giving rise to the Central System, the Iberian Chain, and the Duero and Tajo basins. Finally, the Neogene extension, which mainly affected the eastern and southern parts of the Iberian Peninsula, was responsible for the opening of the Valencia Trough and the Alboran Sea with volcanic activity that lasted until recent times.

This tectonic evolution resulted in conspicuous variations of surface heat flow and crustal and lithospheric thickness, which may result in large departures from a homogeneous elastic Earth model and therefore, in noticeable residuals of the cosine component of the gravity tides. In the next sub-sections, we detail how the structural parameters controlling the lithosphere rheology are calculated in the vicinity of the gravity stations and how the gravity tide residuals have been obtained.

### *2.1 Structural parameters*

Laboratory experiments and rheological studies show that the capability of the lithosphere to be deformed when submitted to external forces depends on its geometry, temperature distribution, and rock composition (Ranalli, 1995). For a given strain rate, lithospheric stiffness is mainly sensitive to surface heat flow such that the higher the heat flow the weaker the lithosphere. Surface heat flow near each gravity tide station is inferred from the heat flow map of the Iberian Peninsula (M. Fernàndez et al., 1998). The reported values vary from 65 ± 10 mW $m^{-2}$ in the central region, to 40 – 50 mW $m^{-2}$ in the Atlantic margin and 80 – 100 mW $m^{-2}$ in the Mediterranean margin, with an average uncertainty of ± 10% or larger. In addition to surface heat flow, we have also considered other structural parametres that are related to lithospheric stiffness such as the tectonothermal age of the lithosphere (the older the stronger), the temperature at the base of the crust (Tmoho) as proposed from the thin sheet lithosphere approach (e.g., Sonder and England, 1986), and the integrated lithospheric strength obtained from stress envelopes (Ranalli, 1995).

In order to assign a tectonothermal age to each gravity tide station, we have distinguished, according to Vergés and Fernàndez (2006), three main geological units that correspond, respectively

to the Hercynian (Devonian to Permian), Intermediate (mainly Mesozoic), and Alpine (Cenozoic) (see Figure 2). The lithospheric thermal structure in each gravity station has been calculated by using a 1D approach which combines surface heat flow and topography data under the assumption of local isostasy (Morgan and M. Fernàndez, 1992). This approach requires knowledge of the densities and thicknesses of the crustal layers and of the lithospheric mantle, as well as the corresponding thermal properties (thermal conductivity and radiogenic heat production values). For the crust, we have distinguished three layers: post Mesozoic sedimentary cover, upper crust, and lower crust whose corresponding thicknesses have been derived from seismic data. Thermal parameters and densities have been taken from direct measurements (M. Fernández et al., 1998) and from literature and are summarized in Table 1. The density of the lithospheric mantle is temperature-dependent and the lithosphere-asthenosphere boundary corresponds to the 1350 ºC isotherm. With this methodology, the Moho temperature is calculated with an uncertainty of ±100 ºC when considering an uncertainty of ±10% in surface heat flow, thermal conductivity and surface heat production, and ±5% in crustal thickness, and average crustal density, and can be reduced to ±70 ºC when uncertainties of ±5% in heat flow and thermal conductivity are considered.

Integrated lithospheric strength is calculated from the concept of strength envelope (Ranalli, 1995) where according to generalized laboratory experiments the deformation regime of a rock can be subdivided into the brittle and ductile domains. Uncertainties in determining the rheological rock parameters are high and can largely affect the absolute values of the calculated lithospheric strength (M. Fernández and Ranalli, 1997). However, we are interested in relative variations of the integrated lithospheric strength and hence, the chosen values of rheological parameters become less critical, though uncertainties in determining the geotherm remain important and even amplified. In our calculations we have considered a quartz upper crust, a diabase/diorite lower crust, and an olivine upper mantle with the rheological parameters given by (Lynch and Morgan, 1990).

The 21 stations of the Iberian gravimetric tide network, with their corresponding latitude and longitude are listed in Table 2. Table 3 shows the surface heat flow and the tectonothermal age for each gravity tide station, as well as the calculated Moho temperature and integrated lithospheric strength that are compatible with the observed mean elevation and crustal structure.

### *2.2 Gravity tide residuals*

To facilitate comparison with previous results, we used in our first approach the Wahr–Dehant Earth model (Dehant, 1987) and the SCHW80 ocean model (Schwiderski, 1980) to obtain the residual vectors of the different gravimetric tide waves considered. All data required to calculate the sine and cosine components of vector **X**, for all combinations of the aforementioned Earth and ocean models and $M_2$ and $O_1$ tidal waves were drawn from the data and results supplied by the ICET.

The Schwiderski model (SCHW80) has been regarded for a long time in geophysics as a working standard for the calculation of the oceanic loading and attraction vector **L** (Melchior, 1994a). It is a numerical model that uses Laplace equations and includes oceanic loading, oceanic mass attraction and friction effects. The main drawback is the low resolution of the mesh (1º x 1º) into which the ocean surface is divided. Many coastal areas are too small to be included and seas such as the Baltic, the Mediterranean or the Sea of Japan do not appear on the global maps either. More recent oceanic models based on TOPEX/POSEIDON satellite altimetry data, e.g., CSR3 (Eanes and Bettadpur, 1996), FES95 (Le Provost et al., 1988) and ORI96 (Melchior and Francis, 1986), match the gravity tide measurements better than SCHW80 (Baker and Bos, 2003). Therefore, in addition to the SCHW80 model, we have also considered the FES 95 model in our study to test the departures between them. It should be mentioned however, that by the moment there is no oceanic tide models that provide satisfactory results for all regions of the world, so local charts must be plotted for specific areas. In the case of the Iberian Peninsula, Iberia charts $M_2$ and Iberia $S_2$ (Vieira et al., 1985a, 1985b), hereinafter referred to as the Iberia charts, exist respectively for tide waves $M_2$ and $S_2$, providing values for the zone $48^{\circ} N \geq \varphi \geq 31^{\circ} N$ ; $8{,}25^{\circ} E \geq \lambda \geq -16^{\circ} W$ . Whereas Schwiderski proposed a mesh of 1º x 1º, the Iberia charts are digitised on a basic scale of 0º.5 x 0º.5, which is reduced to squares of 0º.0625 x 0º.0625 in coastal areas. By replacing these charts in the corresponding area of the global charts of Schwiderski, Vieira et al. (1985a, 1985b) obtained values for vector **L**(L, λ) that we have also used for this study.

For some of the tidal stations, namely Valle de los Caidos, Madrid, Granada and Sepúlveda, there is more than one ICET file because different gravimeters were used. Hence, we considered two data

sets for the Iberian data: Set 1 including the values obtained for the longest time record interval, and Set 2 containing the values corresponding to series with better quality factors $Q_1$ and $Q_2$ (see Table 4 and Appendix). Table 2 incorporates Set 1 and Set 2 and the gravimeters used in every case. Data Set 2 eliminates three of the four Askania stations included in Data Set 1 due to the high noise of this gravimeter compared to LaCoste & Romberg instrument (Baker, 1984).

Table 3 displays the numerical values obtained for the sine and cosine components of the residual vectors for the $M_2$ wave, Wahr-Dehant's Earth model and two ocean tide models used in this study: FES95 and Iberia $M_2$ (SCHW80 supplemented with the Iberia charts for the $M_2$ wave). All data appearing on Table 3 are the best in terms of quality factors $Q_1$ and $Q_2$.

## 3. STUDY OF THE SIGNAL AND NOISE COMPONENTS IN THE GEOPHYSICAL DATA

Both the tidal residual data and the structural parameters contain a certain amount of local noise that cannot be extrapolated to adjoining stations. This noise may be due to observational inaccuracies and, especially, to local effects that have no repercussion on distant stations. Prior to the correlation analysis between different parameters, we determine those correlated signals that can be identified over a given level of noise by means of an autocorrelation analysis. Then, if the data are reduced to uncorrelated noise, the correlogram must be flat and, conversely, if there is a correlated signal, the correlogram must have a characteristic empirical structure (see figures in this section). The least squares prediction (collocation) and covariance analysis consist of the following steps (Moritz, 1980):

1. Breaking down the data vector $\boldsymbol{d}$, corresponding to values $v_i$ on sites $P_i$, as

$$\boldsymbol{d} = \boldsymbol{v} + \boldsymbol{p} = \boldsymbol{s} + \boldsymbol{n} + \boldsymbol{p} \qquad (1)$$

   where $\boldsymbol{p}$ is the systematic part, $\boldsymbol{v}$ is the stationary random component, $\boldsymbol{s}$ is the correlated signal, and $\boldsymbol{n}$ is the uncorrelated noise. Component $\boldsymbol{p}$ can be determined and eliminated through polynomial adjustment.

2. Determination of empirical covariances cov*(d)* for the values of random component $\boldsymbol{v}$ with respect to its mutual distance, *d*.

3. Adjustment of the empirical covariances cov(*d*) by an analytical function C(*d*).

4. Identification of the signal and noise levels. The variance of the signal and is equal to the covariance for zero distance, C(0) and the noise variance will be: $\sigma_n^2 = \sigma^2 - C(0)$, where $\sigma^2$ is the variance for the data ***v***.
5. Calculation of covariance matrixes $\boldsymbol{C}=(C_{ij})$ from the adjusted covariance function:

$$C_{ij} = C(d); \quad d = dist(P_i P_j). \qquad (2)$$

6. Least squares prediction of the signal and data filtering from the covariance matrixes for signal ***s*** and noise ***n***.
7. Calculation of prediction error matrix.

We have conducted this autocorrelation study for the cosine component of the different types of residuals of the $M_2$ and $O_1$ gravimetric tide waves considered (see Tables 2 and 3), which implies four different signal-to-noise studies. To avoid possible misleading results, we have removed those stations with final residuals higher than three times the standard deviation.

First we study data Set 1 and the corresponding final residuals using the ocean tide model SCHW80. The cosine component data of the $M_2$ gravimetric tidal wave contain a significant correlated signal that, in variance, represents 40% of the data magnitude. The main diurnal wave, $O_1$ is seen to be formed almost exclusively by noise (the correlated signal is 5% in variance and is hard to detect). This is due to the fairly lower level of reliability of the tidal residuals with respect to $M_2$ for the same recording period (in the same period of time, the number of data for $O_1$ is the half as much as for $M_2$) and also, to the greater sensitivity with respect to oceanic disturbances. Considering these results we will only use $M_2$ wave in this study. The autocorrelation analyses and least-squares predictions for the tidal residuals $X\cos\chi$ for $M_2$ and $O_1$ are shown in Figs. 3 and 4, respectively. Some stations are markedly anomalous with respect to the general correlated trend. This is case of Sepúlveda for the $M_2$ wave and Porto and Sepúlveda for the $O_1$ wave. This may be due to the presence of parasite local phenomena and may make it advisable not to use them in the correlation studies.

Using the SCHW80 ocean tide model and data Set 2 yields a correlated signal for $M_2$ wave that is barely a 16% of the data magnitude (Figure 5). A possible explanation for those results could be that, at the attainable precision level, gravity tidal residuals would be mainly composed by observational noise and a small fraction of a correlated signal.

Next we use the same data Set 2, but with FES95 ocean tide model instead of SCHW80. In this case the amount of correlated signal for $M_2$ is similar to the previous case (16%) and the magnitude of the tidal residuals decrease around 2% (from 0.334 to 0.326 μGal). This ocean model is more modern and produces a better agreement with the observations and the resulting signal/noise ratio using FES95 is 10% greater than considering SCHW80. For both, SCHW80 and FES95 ocean tide models, the signal follows a covariance function exponential Bessel type (Figure 6).

Finally we consider data Set 2, with SCHW80 supplemented with the Iberia chart for $M_2$ wave. In this last case, the autocorrelation analysis of the residuals indicates a much more random behaviour. The correlated signal detected is just an 8% (Figure 7) indicating that these residuals are nearly random data. The stations of Porto, Oviedo and Túnel del Cadi were not considered in this latest study, because there are no data available for them in the Iberia $M_2$ model.

Next, in order to appraise the results obtained, we conducted the same signal determination study for the heat flow as main structural parameter. For similarity, we consider the data at the same geographical locations as the 21 tidal stations. The correlated signal accounts for 50% of all the data in variance, the rest being attributable to data defects or local effects of the wavelength being smaller than the one determined here by the distribution of stations. Figure 8 displays the adjustment of the analytical function for the empirical autocorrelation values calculated for heat flow. Figure 8 displays also the morphology of the correlated signal and of the errors of the process for the heat flow parameter.

## 4. RESULTS

We have tested linear correlations between the **X** vector cosine component values obtained for the Iberian tide network stations and heat flow, temperature at the base of the crust (Tmoho), integrated lithospheric strength and tectonothermal age values given in Table 3. As described above, we have

first considered the Wahr–Dehant's Earth model and SCHW80 ocean model, and examined its correlation with the cosine component of the final residual for the $M_2$ wave, for both data Sets 1 (CASE A) and 2 (CASE B) (Table 2). The same analysis has been performed using the FES 95 ocean tide model instead of SCHW80 (only Set 2 data this time) (CASE C). Finally, we consider the SCHW80 ocean model supplemented with the Iberia $M_2$ ocean tide chart (as in Table 3) (CASE D). $O_1$ wave has been excluded from this study because of the low presence of correlated signal in the associated residuals. All the obtained results are described in Table 5.

For heat flow and CASE A, the line obtained has a correlation coefficient of R=0.494, close to the value R = 0.598 obtained by Melchior (1995) for Europe using 72 stations. The mean value of 62.02 mW/m$^2$ (for $y$ = 0) is slightly smaller than the average heat flow value for the Iberian Peninsula (65 ± 10 mW/m$^2$). The resultant slope (0.047 μGal/mWm$^{-2}$) is higher than that obtained by Melchior (1995) for Europe (0.0113 μGal/mWm$^{-2}$) and also for Europe plus the rest of the world, excluding South America (0,020 μGal/mWm$^{-2}$). Furthermore, the mean heat flow value for Iberia is rather higher than the values considered by Melchior (1995) (62 instead of 57 mW/m$^2$). It is worth noting that two of the analyzed stations (Sepúlveda and Porto) display out-of-trend values with residuals greater than 1 even when heat flow uncertainties of 10-15 % are considered. Suppression of these two stations makes the slope to be much closer to the values given in Melchior (1995) whereas the intersection occurs at $x$ = 63.41 mW/m$^2$, a closer approach to the mean value for the Iberian Peninsula. CASE B shows a lower correlation coefficient value, R=0.276, being now not significant. For CASE C the results are even worse and the correlation coefficient is quite similar to that reported by Rydelek et al. (1991), who obtained a value of 0.222 after disregarding 56 of the total of 71 stations due to the low signal-to-noise ratio. For CASE D, the correlation coefficient is higher than for CASE C (FES95 model) and the mean value for $y$ = 0 (64.96 mW/m$^2$) matches well with the Iberian average heat flow (65 ± 10 mW/m$^2$). The resulting slope is 0.026 μGal/mWm$^{-2}$. Note that columns under "Iberia M2" title in Table 3 includes only values for 18 stations because there are no **L** vector data for stations Oviedo, Túnel del Cadi and Porto.

For the Tmoho and the lithospheric strength parameters, CASE A shows lower correlation coefficients than for heat flow (Table 5), although the slopes suggest consistent correlations indicating

an increase in tidal residuals for weaker lithospheres. Similarly to heat flow, for all the other cases the correlation coefficients obtained are not significant compared to the standard deviation values. The poorest correlation of these parameters with the gravity tide residuals is related to the fact that both Tmoho and lithospheric strength depends strongly on the measured surface heat flow and additionally, on other rock parameters. This may result in large uncertainties, which in the case of the calculated temperature at the base of the crust (average value of c.a. 540 ºC) lies between ±70 ºC and ±100 ºC. The uncertainties associated with the lithospheric strength can be much larger since the uncertainties in rock rheology parameters must be added.

According to the global data, Melchior (1995) proposes a relation between $M_2$ and the tectonothermal age and justifies that for ages > 800 m.y., the residuals are negative while for regions younger than 250 m.y., the residuals are positive. However, in the Iberian Peninsula all the geological domains are younger than 250 – 300 m.y. and yet the residuals are positive and negative. Only when using ocean tide model FES 95 (Set 2 tidal data) most of the residuals (15 out of 21) are positive, whereas for the Iberia $M_2$ ocean tide model, half of them are positive and the other half are negative.

## 5. DISCUSSION AND CONCLUSIONS

The performed autocorrelation analysis reveals the existence of a correlated signal in the $M_2$ wave tidal residuals that for the SCHW80 ocean tide model and Set 1 tidal data reaches a 40% of the data magnitude. When using Set 2 tidal data and ocean tide models SCHW80 and FES95, the correlated signal decays to 16% and practically disappears when SCHW80 model is complemented with the Iberia $M_2$ local chart. These results suggest that the Iberia $M_2$ oceanic tide model accounts for most of the oceanic effect yielding nearly random tidal residuals.

A significant result of the autocorrelation analysis is that the cosine component of $O_1$ wave is formed almost exclusively by noise for all the tide models and data set analysed. The lack of effects of lateral heterogeneities on the $O_1$ tidal wave is common result in gravity tide studies although the magnitudes of these effects should be similar for both $O_1$ and $M_2$ waves (Baker and Bos, 2003).

The analysis of correlation between the $M_2$ tide wave residuals and structural parameters such as heal flow, Moho temperature, lithospheric strength and tectonothermal age shows a similar pattern to

that obtained from the autocorrelation study. Therefore, when using the SCHW80 ocean model and Set 1 tidal data, the results show a consistent correlation such that the weaker the lithosphere the higher the tide residuals. This is especially evident for the measured surface heat flow with results very similar to those obtained independently by Melchior (1995) for all Europe and in global studies. Clearly, the parameter that better correlates with tidal residuals is the surface heat flow since it is a direct measure and therefore less affected by uncertainties in other rock or structural parameters.

However, after rejecting poor quality stations, i.e. using Set 2 tidal data, and including more accurate ocean tide models (FES95) and local models (Iberia $M_2$), the correlation with structural parameters is poorest becoming mainly noise. These results would confirm the conclusions suggested by Rydelek et al. (1991) who propose that the large uncertainties associated with the measurements of both gravity tides and structural parameters mask any possible relationship between them and makes uncertain any empirical correlation.

Finally, our results for the Iberian Peninsula agree with theoretical studies that conclude that distortions of the tidal gravity field by local, regional and even large scale deviations of an homogeneous elastic Earth are very small and then hardly to observe with the presently available instrumentation. In contrast, the tidal deformation field measured with tiltmeters and strainmeters appears heavily distorted by local heterogeneities (Harrison, 1985; Zürn, 1997). Following Beaumont and Berger (1974), regions with active seismicity could show easily measurable transient modification of the tidal tilt and strain amplitude under certain stress conditions. According to these authors, the tidal tilt and strain amplitudes may be affected by up to 50% of variation within a distance of one or two scale lengths from the discontinuity (fault). This could be the case of the southern and north and northwestern parts of the Iberian Peninsula which are characterized by active seismicity (Buforn et al., 1995; Souriau and Pauchet, 1998; Martinez-Diaz et al., 2006). Unfortunately, not enough data of this type are presently available in the Iberian Peninsula to confirm conclusions.

**Acknowledgments**. The research by JF, LM and AGC has been funded under MCyT projects REN2002-03450 and CGL2005-05500-C02. The research by AGC has been also partially funded under DGIMCT project HP2001-0081. The research by MF has been funded through MCyT projects

REN2001-3868-C03-02/MAR, REN2002-11230-E-MAR (ESF-EuroMARGINS 01-LEC-EMA22F) and TopoIberia Consolider-Ingenio 2010 nº CSD 2006-00041. We would like to acknowledge the ICET and B. Ducarme for giving us the analysis results from the gravity tide data of the Iberian Peninsula existing in the ICET databank. We thank an anonymous reviewer and G. Ranalli for their useful suggestions to improve the quality of this manuscript.

***APPENDIX: On quality factors and calibrations***

All files from the ICET show the standard deviations of the diurnal (D) and semidiurnal (SD) bandwidths for every station. According to Chueca (1991), these values reflect different types of errors, including calibration, signal to noise ratio and instrumental sensitivity to external perturbations such as atmospheric pressure and temperature. Chueca et al. (1985) use these standard deviations D and SD to define two quality factors for every series of observations, reflecting both internal errors and station efficiency:

$$Q_1 = \frac{10R}{\sqrt{D \cdot S}}(1+P)$$

$$Q_2 = \frac{R}{\sqrt{E(O_1) \cdot E(M_2)}}$$

with

R = station efficiency = (number of readings/24 x time interval in days)

D = diurnal band standard deviation

S = semidiurnal band standard deviation

$E(O_1)$ = squared mean error for $O_1$ estimated amplitude

$E(M_2)$ = squared mean error for $M_2$ estimated amplitude

P = weight of the series, being equal to 0 if there is no separation in wave group $P_1S_1K_1$, and equal to 1 if wave group $P_1$ has been separated from $S_1K_1$.

Quality factors depend to a great extent on the type of instrument used. Table 4 presents $Q_1$ and $Q_2$ global means for different kinds of gravimeters (adapted from Chueca 1991). Lowest values are for Askania 11 and 12, featuring quality factors $Q_1 = 0.9$ and $Q_2 = 3.2$, while the highest values are for superconducting instruments, with quality factors beyond 100.0. It is clear that high $Q_1$ and $Q_2$ values correspond to good series performed with gravimeters delivering a high signal to noise ratio. Quality factors $Q_1$ and $Q_2$ are present in all ICET files used in this paper, and they are showed in Table 3, with the "normalization factors" relative to calibration (see Melchior, 1994b).

**REFERENCES**

Arnoso, J., Fernández, J. and Vieira, R., 2001. Interpretation of tidal gravity anomalies in Lanzarote, Canary Islands. J. of Geodynamics, 31: 341 – 354.

Badal, J., Corchete, V., Payo, G., Pujades, L., Canas, J.A., 1996. Imaging of shear – wave velocity structure beneath Iberia. Geophys. J. Int., 124: 591 – 611.

Baker, T.F., 1984. Tidal deformations of the Earth. Sci. Prog., Oxf., 69, 197-233.

Baker, T. F. and Bos, M. S., 2003. Validating Earth and ocean tide models using tidal gravity measurements. Geophys. J. Int., 152: 468 – 485.

Banda, E., 1988. Crustal parameters in the Iberian Peninsula. Phys. Earth. Planet. Inter., 51:222–225.

Beaumont, C. and Berger, J., 1974. Earthquake Prediction: Modification of Earth Tide Tilts and Strains by Dilatancy. Geophys. J. R. Astr. Soc. 39: 111 – 118.

Burforn, E., Sanz de Galdeano, C., Udías, A., 1995. Seismotectonic of the Ibero-Maghrebian region. Tectonophysics, 248, 247-261.

Camacho, A.G, Vieira, R, 1990. Predicción de la corrección de marea en la Peninsula Ibérica. Física de la Tierra, 2, 87-110.

Chueca, R., 1991. Método de obtención del efecto oceánico indirecto de pequeños armónicos no considerados en los modelos oceánicos existentes. Aplicación a $L_2$. PhD Thesis, Universidad Complutense de Madrid.

Chueca, R., Ducarme, B. and Melchior, P., 1985. Preliminary investigation about a quality factor of tidal gravity stations. Bull. Inf. Marées Terrestres, 94, 6334 – 6337.

Dehant, V., 1987. Tidal parameters for an inelastic Earth. Phys. Earth Planet. Inter. 49: 97–116.

Dehant, V., Defraigne, P. and Wahr, J.M., 1999. Tides for a convective Earth. J. Geophys. Res., 104, 1035-1058.

Eanes, R. J. and Bettadpur, S., 1996. The CSR3.0 Global Ocean Tide Model: Diurnal and Semi – Diurnal Ocean Tides from TOPEX/POSEIDON Altimetry. CSR – TM – 96 – 05, The University of Texas Center for Space Research.

Fernández, J., Vieira, R., Díez, J.L. and Toro, C., 1992. Investigation on crustal thickness, heat flow and gravity tide relationship in Lanzarote Island. Phys. Earth Planet. Inter., 74: 199 – 208.

Fernández, M. and Ranalli, G., 1997. The role of rheology in extensional basin formation modelling. Tectonophysics, 282: 129-145.

Fernández, M., Marzán, I., Correia, A. and Ramalho, E., 1998. Heat flow, heat production, and lithospheric thermal regime in the Iberian Peninsula. Tectonophysics 291: 29 – 53.

Harrison, J.C. (ed.), 1985. Earth Tides. In: Benchmark Papers in Geology Series. pp. 1 – 419. Van Nostrand Reinhold, New York.

Herrin, E. and Taggart, J., 1962. Regional variations in $P_n$ velocity and their effect on the location of epicentres. Bull. Seismol. Soc. Am., 52: 1037 – 1046.

Hinderer, J. and Crossley, D., 2000. Time variations in gravity and inferences on the Earth's structure and dynamics. Surv. Geophys., 21: 1 – 45.

Jeligovski, V. A., Melchior, P. and Sadovskii, A. H., 1988. Anomalies de marées, flux thermique et séismicité. Probl. Seismol. Informatiki, Moscou, 21: 32 – 37.

Le Provost, C., Lyard, F., Molines, J. M., Genco, M. L. and Rabilloud, F., 1998. A hydrodynamic ocean tide model improved by assimilating a satellite altimeter derived data set. J. Geophys. Res. 103: 5513 – 5529.

Lynch, H.D. and Morgan, P., 1990. Finite element models of continental extension. Tectonophysics, 174: 115-135.

Mantovani, M.S.M., Shukowsky, W., de Freitas, S.R.C. and Brito Neves, B.B., 2005. Lithosphere mechanical behavior inferred from tidal gravity anomalies: a comparison of Africa and South America. Earth Planet. Sci. Lett., 230: 397-412.

Martínez-Díaz, J.J., Capote, R., Tsige, M., Villamor, P., Martín-González, F., Insua-Arévalo, J.M., 2006. Seismic triggering in a stable continental area: The Lugo 1995-1997 seismic sequences (NW Spain). Journal of Geodynamics, 41, 440-449.

Melchior, P., 1983. The tides of the planet Earth. Pergamon, Oxford, 2nded., p. 641.

Melchior, P., 1994a. A new data bank for tidal gravity measurements (DB 92). Phys. Earth Planet. Inter., 82: 125 – 155.

Melchior, P., 1994b. Checking and correcting the tidal gravity parameters of the ICET Data Bank. Bull. Inf. Marées Terrestres, 119, 8899 – 8936.

Melchior, P., 1995. A continuing discussion about the correlation of tidal gravity anomalies and heat flow densities. Phys. Earth Planet. Inter., 88: 223 – 256.

Melchior, P. and De Becker, M., 1983. A discussion of worldwide measurements of tidal gravity respect to oceanic interactions, lithosphere hetereogeneities, Earth flattening and inertial forces. Phys. Earth Planet. Inter., 31: 27 –53.

Melchior, P. and Ducarme, B., 1991. Tidal gravity anomalies and tectonics. In: Proceedings 11th International Symposium on Earth Tides (Kakkuri, J., ed.), Helsinki, pp. 445 – 454.

Melchior, P. and Francis, O., 1986. Comparison of recent ocean tide models using ground – based tidal gravity measurements. Marine Geodesy, 19: 291 – 330.

Melchior, P., Ducarme, B. and De Becker, M., 1986. Corrélation entre le flux de chaleur et les déformations radiales de marée terrestre en Afrique. INQUA, Dakar Symposium, Changements globaux en Afrique, pp. 305 – 308.

Molodenskii, S.M. and Kramer, M.V., 1980. The influence of large-scale horizontal inhomogeneities in the mantle on earth tides. Bull. Acad. Sci. USSR, Earth Phys., 16: 1 – 11.

Morgan, P. and Fernàndez, M., 1992. Neogene vertical movements and constraints on extension in the Catalan Coastal Ranges, Iberian Peninsula, and the Valencia trough (western Mediterranean). Tectonophysics, 203: 185-201.

Moritz, H., 1980. Advanced Physical Geodesy, Herbert Wichmann Verlag, ed., Karlsruhe, Germany, 500 pp.

Ranalli, G., 1995. Rheology of the Earth. Chapman and Hall, London, 2nd. ed., 413 pp.

Robinson, E. S., 1989. Tidal gravity, heat flow and the upper crust. Phys. Earth Planet. Inter., 56: 181 – 185.

Robinson, E. S., 1991. Correlation of tidal gravity and heat flow in eastern North America. Phys. Earth Planet. Inter., 67: 231 – 236.

Robinson, E. S., 1993. On tidal gravity, heat flow and lateral heterogeneities – Comment. Phys. Earth Planet. Inter., 76: 343 – 346.

Rydelek, P. A., Zürn, W. and Hinderer, J., 1991. On tidal gravity, heat flow and lateral hetereogeneities. Phys. Earth Planet. Inter., 68: 215 – 229.

Schwiderski, E., 1980. On charting global ocean tides. Rev. Geophys. Space Phys. 18: 243–268.

Shukowsky, W. and Mantovani, M.S.M., 1999. Spatial variability of tidal gravity anomalies and its correlation with the effective elastic thickness of the lithosphere. Phys. Earth Planet. Int., 114: 81-90.

Sonder, L.J., and England, P.C., 1986. Vertical averages of rheology of the continental lithosphere: Relation to thin sheet parameters. Earth Planet. Sci. Lett., 77: 81-90.

Souriau, A. and Pauchet, H., 1998. A new synthesis of Pyrenean seismicity and its tectonic implications. Tectonophysics, 290, 221-244.

Torné, M., Fernández, M., Comas, M.C. and Soto, J.I., 2000. Lithospheric strcuture beneath the Alboran basin: Results from 3D gravity modelling and tectonic relevance. J. Geophys. Res., 105, 3209-3228.

Vera, J.A. (editor), 2004. Geología de España. SGE-IGME, Madrid, 890 pp.

Vergés, J. and Fernàndez, M., 2006. Mountain Ranges and Basins in the Iberian Peninsula. In: D. Gee and R. Stephenson Eds. European Lithosphere Dynamics. Geological Society London Memoir , 32, 223-234, 2006.

Vieira, R., Toro, C. and Megias, E., 1985a. Ocean tides in the nearby of the Iberian Peninsula. Part I: M2 Iberia Map. Proceedings Tenth International Symposium on Earth Tides. Consejo Sup. Investigaciones Científicas, Madrid, pp. 679 – 695.

Vieira, R., Toro, C. and Fernández, J., 1985b. Ocean tides in the nearby of the Iberian Peninsula. Part II: S2 Iberia Map. Proceedings Tenth International Symposium on Earth Tides. Consejo Sup. Investigaciones Científicas, Madrid, pp. 697 – 706.

Wang, R., 1991. Tidal deformations on a rotating, spherically asymmetric, visco-elastic and laterally heterogeneous Earth. PhD thesis, European University Studies, Series XVII, Earth Sciences, Vol. 5, Peter Lang, Frankfurt am Main, p. 139.

Yanshin, A. L., Mechior, P., Keilis – Borok, V.I., De Becker, M., Ducarme, B. and Sadovsky, A. M., 1986. Global distribution of tidal anomalies and an attempt of its geotectonic interpretation. Proceedings 10$^{th}$ International Symposium on Earth Tides (Vieira, R., ed.), Madrid, pp. 731 – 755.

Zeyen, H. and Fernández, M., 1994. Integrated lithospheric modeling combining thermal, gravity and local isostasy analysis: Application to the NE Spanish Geotransect. J. Geophys. Res., 99: 18089 – 18102.

Zürn, W., 1997. Earth tide observations and interpretation. In: H. Wilhelm, W. Zürn, and H.-G. Wenzel (Eds.), Tidal Phenomena, Lecture Notes in Earth Sciences, 66, 77-94.

Zürn, W., Beaumont, C. and Slichter, L.B., 1976. Gravity tides and ocean loading in southern Alaska. J. Geophys. Res., 81: 4923 – 4932.

**FIGURE CAPTIONS**

**Figure 1.** Graphical representation of the final residual vector (**X**), observed residual vector (**B**), computed oceanic loading and attraction vector (**L**), observed vector (**A**) and body tide vector (**R**) (Arnoso et al., 2001).

**Figure 2.** Location of the 21 tidal stations used in this study and indication of their tectonothermal domain (Hercynian, Intermediate, and Alpine). See Table 2 for coordinates and the corresponding ICET numbering. Geological basemap modified from Vergés and M. Fernàndez (2006).

**Figure 3.** Analysis of autocorrelation and least-squares prediction for the tidal residuals Xcos$\chi$ for $M_2$, in accordance with Wahr-Dehant's Earth model and ocean model SCHW80 and the tidal data set 1 (Table 2), in the Iberian peninsula (without Sepulveda station). **(a)** empirical autocorrelation values and adjusted autocorrelation function (correlation step 67'), the correlated signal reaches 40% in variance showing a high presence of some effects superimposed to a noncorrelated noise, **(b)** predicted signal (μGal), **(c)** prediction error (μGal).

**Figure 4.** Analysis of autocorrelation and least-squares prediction for the tidal residuals Xcos$\chi$ for $O_1$, in accordance with Wahr-Dehant's Earth model and ocean model SCHW80 and the tidal data set 1 (Table 2), in the Iberian peninsula (without Porto station). **(a)** empirical autocorrelation values and adjusted autocorrelation function (correlation step 64'), it shows that data is composed by nearly uncorrelated noise without further correlated effects , **(b)** predicted signal (μGal), **(c)** prediction error (μGal).

**Figure 5.** Analysis of autocorrelation and least-squares prediction for the tidal residuals Xcos$\chi$ for $M_2$, in accordance with Wahr-Dehant's Earth model and ocean model SCHW80 and the tidal data Set 2 (Table 2), in the Iberian peninsula (without Porto station). **(a)** empirical autocorrelation values and adjusted autocorrelation function (correlation step 64'), the correlated signal reach 18% in variance showing a low presence of some effects superimposed to a uncorrelated noise, **(b)** predicted signal (μGal), **(c)** prediction error (μGal).

**Figure 6.** Analysis of autocorrelation and least-squares prediction for the tidal residuals Xcos$\chi$ for $M_2$, in accordance with Wahr-Dehant's Earth model and ocean model FES95 and the tidal data Set 2 (Table

3), in the Iberian peninsula (without Porto station). **(a)** empirical autocorrelation values and adjusted autocorrelation function (correlation step 64'), the correlated signal reaches 18% in variance showing a low presence of some effects superimposed to a uncorrelated noise, **(b)** predicted signal (μGal), **(c)** prediction error (μGal).

**Figure 7.** Analysis of autocorrelation for the tidal residuals Xcosχ for $M_2$, in accordance with Wahr-Dehant's Earth model and ocean model SCHW80 supplemented with the Iberian-$M_2$ chart and the tidal data Set 2 (Table 3), in the Iberian peninsula (without Porto station). Empirical autocorrelation values and adjusted autocorrelation function (correlation step 64'). The analysis provides a non-significant presence of signal, showing a pattern of uncorrelated noise for the tidal residuals.

**Figure 8.** Comparative analysis of autocorrelation and least-squares prediction for the scatered data of Heat Flow ($mW/m^2$) in the Iberian tidal stations (Table 3), in the Iberian peninsula. **(a)** empirical autocorrelation values and adjusted autocorrelation function (correlation step 52'), the correlated signal reaches 50% in variance showing a high presence of some effects superimposed to a uncorrelated noise, **(b)** predicted signal, **(c)** prediction error.

| | Density (kg / m$^3$) | Thermal conductivity (W / m K) | Heat production (μW / m$^3$) |
|---|---|---|---|
| **Sediments** | 2400 – 2650 | 2.4 – 2.5 | 1 |
| **Upper crust** | 2720 – 2770 | 3.0 | 2 – 3 exp(z/15000) |
| **Lower crust** | 2950 | 2.1 | 0.2 |
| **Upper mantle** | 3200 (1+α(Ta-T(z))) | 3.4 | 0.02 |

**Table 1.** Parameters used in thermal calculations. α is the thermal expansion coefficient (3.5 $10^{-5}$ ºC$^{-1}$), Ta is the temperature at the base of the lithosphere (1350 ºC) and T(z) is the temperature at depth z (meters).

| ICET code | Station | Latit N | Long W | M2 SCHW80 (set 1) µGal | | O1 SCHW80 (set 1) µGal | | M2 SCHW80 (set 2) µGal | | O1 SCHW80 (set 2) µGal | | Gravimeter (set 1) | Gravimeter (set 2) |
|---|---|---|---|---|---|---|---|---|---|---|---|---|---|
| | | degrees | | Xcosx | Xsinx | Xcosx | Xsinx | Xcosx | Xsinx | Xcosx | Xsinx | | |
| 401 | Valle Los Caídos | 40.642 | 4.155 | 0.589 | 0.211 | 0.224 | 0.034 | -0.111 | 0.264 | -0.107 | 0.049 | ASK GS-15 | LCR ET-15 |
| 406 | SanFernando | 36.462 | 6.205 | -0.55 | 0.506 | -0.133 | 0.567 | -0.55 | 0.506 | -0.133 | 0.567 | LCR 434 | LCR 434 |
| 402 | MadridFacul. | 40.452 | 3.724 | 0.133 | -0.385 | -0.117 | -0.052 | 0.096 | 0.045 | 0.036 | -0.060 | ASK GS-15 | LCR G-665 |
| 414 | La Granja | 40.899 | 4.004 | -0.375 | 0.283 | -0.528 | 0.154 | -0.375 | 0.283 | -0.528 | 0.154 | LCR 301 | LCR 301 |
| 411 | Barcelona | 41.503 | -2.089 | 0.129 | -0.094 | -0.451 | 0.299 | 0.129 | -0.094 | -0.451 | 0.299 | LCR 301 | LCR 301 |
| 412 | Carbonero | 41.122 | 4.267 | -0.053 | -0.068 | 0.033 | -0.071 | -0.053 | -0.068 | 0.033 | -0.071 | LCR 434 | LCR 434 |
| 405 | Burgos | 42.341 | 3.705 | 0.572 | -0.168 | -0.228 | -0.183 | 0.572 | -0.168 | -0.228 | -0.183 | ASK GS-15 | ASK GS-15 |
| 404 | Santander | 43.466 | 3.807 | -0.017 | -0.097 | -0.687 | 0.277 | -0.017 | -0.097 | -0.687 | 0.277 | LCR 434 | LCR 434 |
| 409 | Cubillos | 41.574 | 5.74 | -0.104 | 0.288 | -0.344 | 0.141 | -0.104 | 0.288 | -0.344 | 0.141 | LCR 301 | LCR 301 |
| 427 | Santiago | 42.881 | 8.545 | 0.586 | 0.782 | 0.396 | 0.097 | 0.586 | 0.782 | 0.396 | 0.097 | LCR 301 | LCR 301 |
| 417 | Arcas | 39.988 | 2.115 | 0.293 | -0.152 | -0.226 | -0.343 | 0.293 | -0.152 | -0.226 | -0.343 | LCR 434 | LCR 434 |
| 413 | Ciudad Real | 38.986 | 3.931 | -0.152 | 0.073 | -0.58 | 0.349 | -0.152 | 0.073 | -0.58 | 0.349 | LCR 301 | LCR 301 |
| 433 | Calatayud | 41.35 | 1.644 | -0.17 | -0.133 | -0.422 | 0.253 | -0.17 | -0.133 | -0.422 | 0.253 | LCR 301 | LCR 301 |
| 407 | Sepúlveda | 41.299 | 3.759 | 1.383 | -1.64 | 0.462 | -0.439 | -0.436 | 0.282 | -0.521 | 0.297 | ASK GS-15 | LCR 301 |
| 434 | Oviedo | 43.35 | 5.85 | -0.155 | 1.291 | 0.08 | 0.036 | -0.155 | 1.291 | 0.08 | 0.036 | LCR 434 | LCR 434 |
| 403 | Granada | 37.187 | 3.592 | 0.113 | 0.444 | -0.144 | 0.184 | 0.113 | 0.444 | -0.144 | 0.184 | LCR 301 | LCR 301 |
| 420 | Pamplona | 42.806 | 1.669 | 0.259 | -0.763 | -0.09 | -0.331 | 0.259 | -0.763 | -0.09 | -0.331 | LCR 434 | LCR 434 |
| 419 | Plasencia | 40.029 | 6.092 | -0.14 | -0.214 | -0.341 | -0.002 | -0.14 | -0.214 | -0.341 | -0.002 | LCR 434 | LCR 434 |
| 424 | Túnel del Cadi | 42.283 | -1.85 | 0.501 | -0.444 | 0.482 | 0.079 | 0.501 | -0.444 | 0.482 | 0.079 | LCR G-665 | LCR G-665 |
| 480 | Porto | 41.08 | 8.67 | 1.017 | -1.553 | 1.511 | -1.778 | 1.017 | -1.553 | 1.511 | -1.778 | LCR G-258 | LCR G-258 |
| 410 | Toledo | 39.86 | 4.01 | -0.604 | -0.29 | -0.887 | 0.426 | -0.604 | -0.29 | -0.887 | 0.426 | LCR 301 | LCR 301 |

**Table 2.** The 21 stations of the Iberian gravimetric tide network, with their corresponding details: latitude, longitude, and the components of the final residual, Xcos$\chi$ and Xsen$\chi$, for the $M_2$ and $O_1$ waves, in accordance with Wahr-Dehant's Earth model and ocean model SCHW80 and both tidal data sets 1 and 2. Gravimeters used are also in the list.

| ICET code | Station | **Elev.** m a.s.l. | Thickness Crust/ Lithosph. km | Tectono-thermal Unit | Heat Flow $mW/m^2$ | Tmoho °C | **Lithos. Strength** $10^{12}N/m$ | M2 (FES95) µGal | | Iberia M2 µGal | | Q1 | Q2 | Normaliz Factor |
|---|---|---|---|---|---|---|---|---|---|---|---|---|---|---|
| | | | | | | | | Xcosx | Xsinx | Xcosx | Xsinx | | | |
| 401 | Valle Los Caídos | 1035 | 34 / 100 | Intermediate | 70 | 608 | 44.6 | 0.02 | 0.267 | -0.029 | 0.079 | 11.1 | 21.8 | 1.01044 |
| 406 | SanFernando | 4 | 30 / 137 | Alpine | 50 | 426 | 115.7 | -0.115 | 0.908 | -0.521 | 1.293 | 2.3 | 5.4 | 0.93898 |
| 402 | MadridFacul | 735 | 32 / 96 | Intermediate | 70 | 593 | 44.5 | 0.216 | 0.057 | 0.171 | -0.116 | 14.0 | 35.7 | 1.00000 |
| 414 | La Granja | 1110 | 34 / 98 | Intermediate | 65 | 602 | 45.5 | -0.253 | 0.292 | -0.311 | 0.096 | 2.1 | 7.6 | 0.96881 |
| 411 | Barcelona | 235 | 28 / 92 | Alpine | 70 | 349 | 47.5 | 0.074 | 0.079 | 0.035 | -0.114 | 4.2 | 7.7 | 0.96881 |
| 412 | Carbonero | 920 | 32 / 93 | Intermediate | 70 | 607 | 39.4 | 0.073 | -0.064 | 0.007 | -0.266 | 2.8 | 6.8 | 0.96988 |
| 405 | Burgos | 935 | 34 / 101 | Intermediate | 67 | 606 | 45.6 | 0.678 | -0.106 | 0.502 | -0.292 | 1.7 | 5.8 | 0.99126 |
| 404 | Santander | 0 | 30 / 118 | Alpine | 58 | 480 | 84.3 | -0.113 | 2.06 | -0.586 | 2.322 | 2.0 | 6.1 | 0.93898 |
| 409 | Cubillos | 725 | 32 / 103 | Hercyinian | 65 | 558 | 55.5 | 0.066 | 0.239 | -0.004 | -0.009 | 11.6 | 19.4 | 0.96881 |
| 427 | Santiago | 300 | 31 / 114 | Hercyinian | 65 | 504 | 75.5 | 0.892 | 0.752 | 0.805 | 0.391 | 2.4 | 9.3 | 0.96881 |
| 417 | Arcas | 1070 | 34 / 103 | Intermediate | 65 | 598 | 48.1 | 0.376 | -0.123 | 0.346 | -0.297 | 1.2 | 4.2 | 0.96988 |
| 413 | Ciudad Real | 685 | 32 / 103 | Hercyinian | 65 | 562 | 54.3 | 0.005 | 0.071 | -0.006 | -0.077 | 3.1 | 10.5 | 0.96881 |
| 433 | Calatayud | 665 | 35 / 123 | Intermediate | 65 | 551 | 74.5 | -0.104 | -0.097 | -0.208 | -0.238 | 7.8 | 16.9 | 0.96881 |
| 407 | Sepúlveda | 1065 | 34 / 104 | Intermediate | 70 | 595 | 49.4 | -0.323 | 0.298 | -0.404 | 0.098 | 2.0 | 5.3 | 0.96881 |
| 434 | Oviedo | 350 | 40 / 162 | Alpine | 57 | 485 | 115.7 | 0.05 | 0.777 | | | 6.4 | 11.9 | 0.99203 |
| 403 | Granada | 1120 | 35 / 117 | Alpine | 65 | 556 | 68.2 | 0.385 | 0.345 | 0.384 | 0.228 | 3.9 | 11.5 | 0.96881 |
| 420 | Pamplona | 650 | 39 / 155 | Alpine | 60 | 517 | 104.9 | 0.359 | -0.723 | 0.148 | -0.940 | 4.3 | 9.7 | 0.96988 |
| 419 | Plasencia | 490 | 32 / 117 | Hercyinian | 65 | 507 | 77.3 | 0.085 | -0.256 | 0.045 | -0.422 | 8.0 | 16.2 | 0.96988 |
| 424 | Túnel del Cadi | 1180 | 40 / 140 | Alpine | 62 | 566 | 84.3 | 0.488 | -0.3 | | | 5.0 | 7.0 | 0.99270 |
| 480 | Porto | 65 | 29 / 110 | Hercyinian | 70 | 495 | 73.2 | 1.678 | -1.987 | | | | | |
| 410 | Toledo | 615 | 32 / 108 | Hercyinian | 65 | 543 | 62.7 | -0.466 | -0.284 | -0.492 | -0.453 | 0.7 | 2.1 | 0.96881 |

**Table 3.** The 21 stations of the Iberian gravimetric tide network, with their corresponding details: elevation, heat flow, crust and lithosphere thickness, tectonothermal age, temperature at the base of the Moho, mean lithospheric strength, and the quality factors $Q_1$ and $Q_2$. The table also lists the data of the components of final residual, Xcosχ and Xsenχ, for $M_2$ wave, in accordance with Wahr-Dehant's Earth model and ocean models FES95 and SCHW80 (this one supplemented with the Iberian chart for the $M_2$ wave). All recordings were performed with LaCoste & Romberg gravimeters, except for the case of the Burgos station, where an Askania GS 15 was used. There are no data about quality factors in the Porto station. Normalization factor F is also included (ICET data).

| Type of instrument | $Q_1$ | $Q_2$ |
|---|---|---|
| Askania 11, 12 | 0.9 | 3.2 |
| Askania 15, BN | 4.2 | 9.4 |
| Geodynamics | 6.2 | 10.2 |
| LaCoste Romberg G, D | 3.6 | 6.5 |
| LaCoste Romberg ET | 13.1 | 22.1 |
| Superconducting | 106.2 | 200.0 |

**Table 4.** Global means of $Q_1$ and $Q_2$ for different kinds of gravimeters (adapted from Chueca 1991).

| | Regression line y=A+Bx | | Correlation Coefficient | Standard Deviation | Value for y=0 |
|---|---|---|---|---|---|
| | A | B | | | |
| | *μGal* | *μGal/(unit)* | | *μGal* | *(unit)* |
| **Heat Flow** *(unit=mW m$^{-2}$)* | | | | | |
| CASE A | -2.915 | 0.047 | 0.494 | 0.42 | 62.02 |
| CASE A' | -1.712 | 0.027 | 0.384 | 0.33 | 63.41 |
| CASE B | -1.369 | 0.022 | 0.276 | 0.38 | 62.23 |
| CASE C | -1.049 | 0.019 | 0.209 | 0.45 | 55.21 |
| CASE D | -1.689 | 0.026 | 0.345 | 0.34 | 64.96 |
| **Tmoho (***unit=$^{o}$C)* | | | | | |
| CASE A | -0.697 | 0.0016 | 0.215 | 0.47 | 435.6 |
| CASE A' | -0.644 | 0.0013 | 0.243 | 0.34 | 495.4 |
| CASE B | 0.106 | -0.00014 | -0.022 | 0.39 | 757.1 |
| CASE C | 0.441 | -0.0005 | -0.065 | 0.46 | 882.0 |
| CASE D | -0.498 | 0.0009 | 0.17 | 0.36 | 553.3 |
| **Lithos. Strength** *(unit=10$^{12}$N/m)* | | | | | |
| CASE A | 0.479 | -0.0048 | -0.231 | 0.47 | 99.79 |
| CASE A' | 0.270 | -0.0033 | -0.225 | 0.34 | 81.82 |
| CASE B | 0.061 | -0.0004 | -0.024 | 0.39 | 152.5 |
| CASE C | -0.093 | 0.0015 | 0.075 | 0.46 | 62.0 |
| CASE D | 0.222 | -0.0036 | -0.212 | 0.36 | 61.67 |

**Table 5.** Results from the regression analysis for gravity residuals with respect to other geophysical magnitudes. The regression line is given by y=A+Bx, where y is the gravity residual value in μGal and x the corresponding parameter expressed in the appropriate units. CASE A corresponds to SCHW80 ocean model and Data Set 1. CASE A' is similar to A but removing stations Sepulveda and Porto. CASE B corresponds to SCHW80 and Data Set 2. CASE C corresponds to Data Set 2 and FES 95 ocean model. CASE D corresponds to Data Set 2 and SCHW80 supplemented with the Iberia chart.

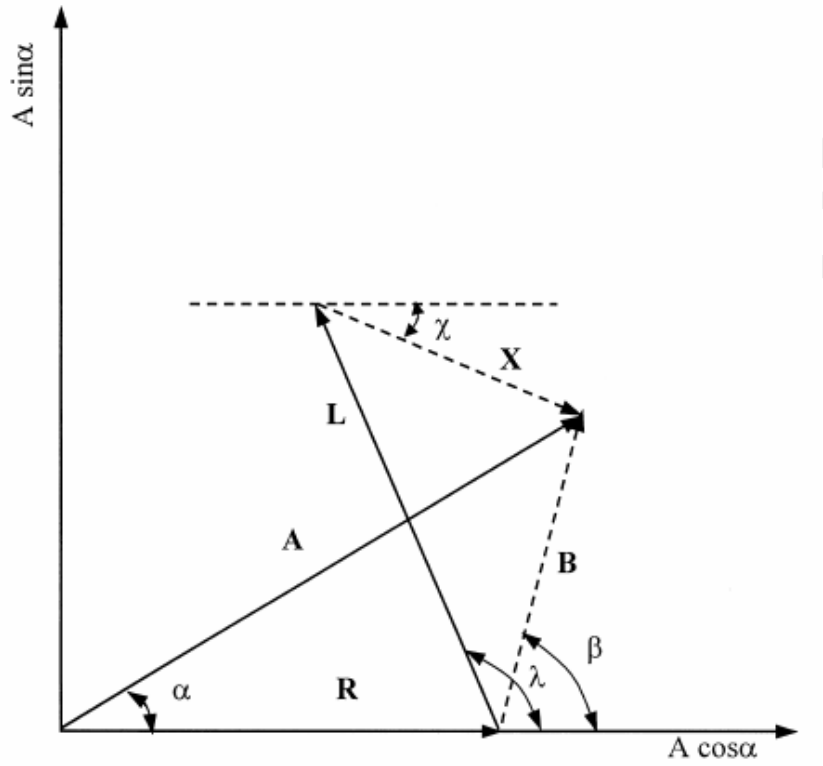


**Figure 1**

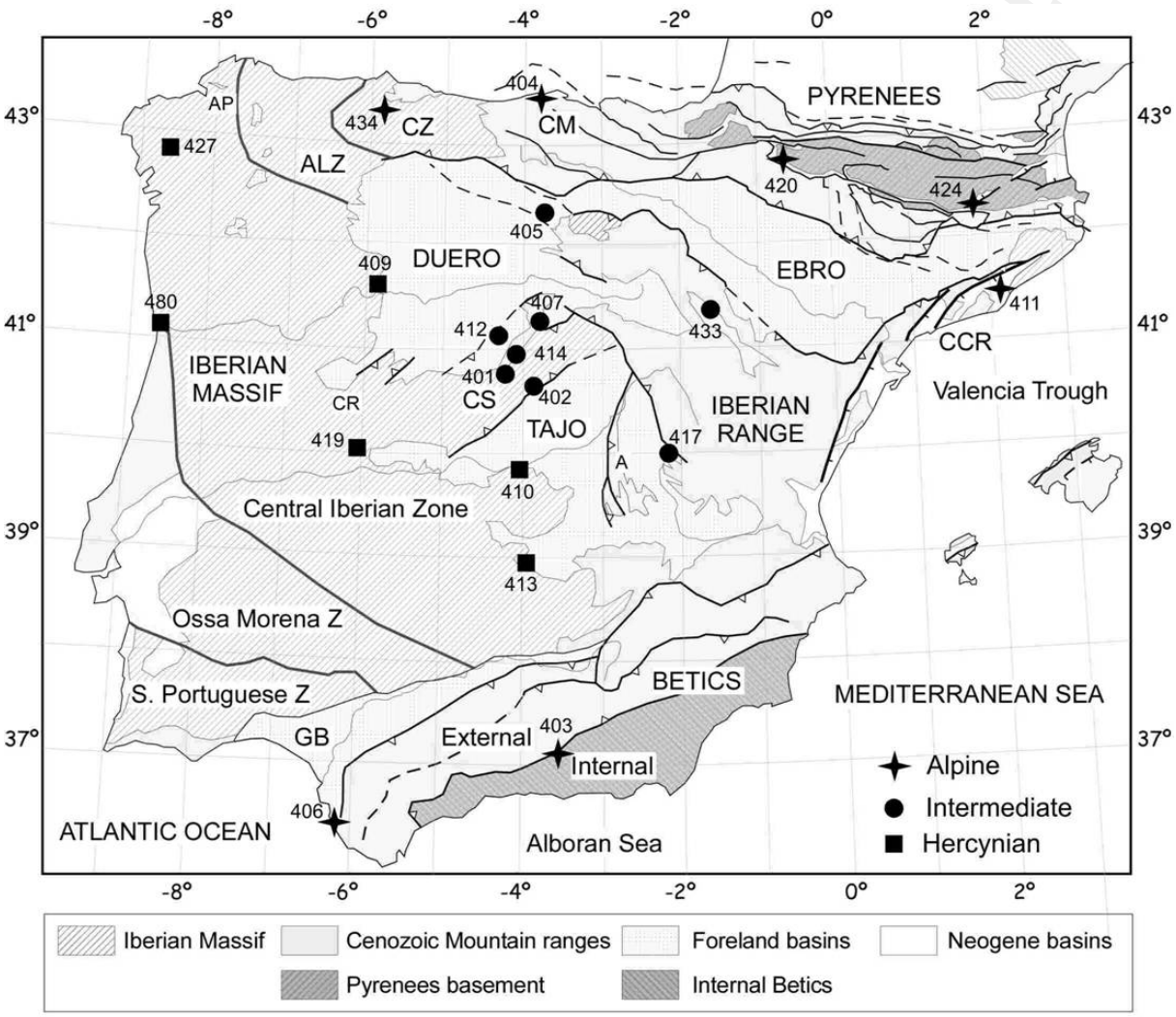


**Figure 2**

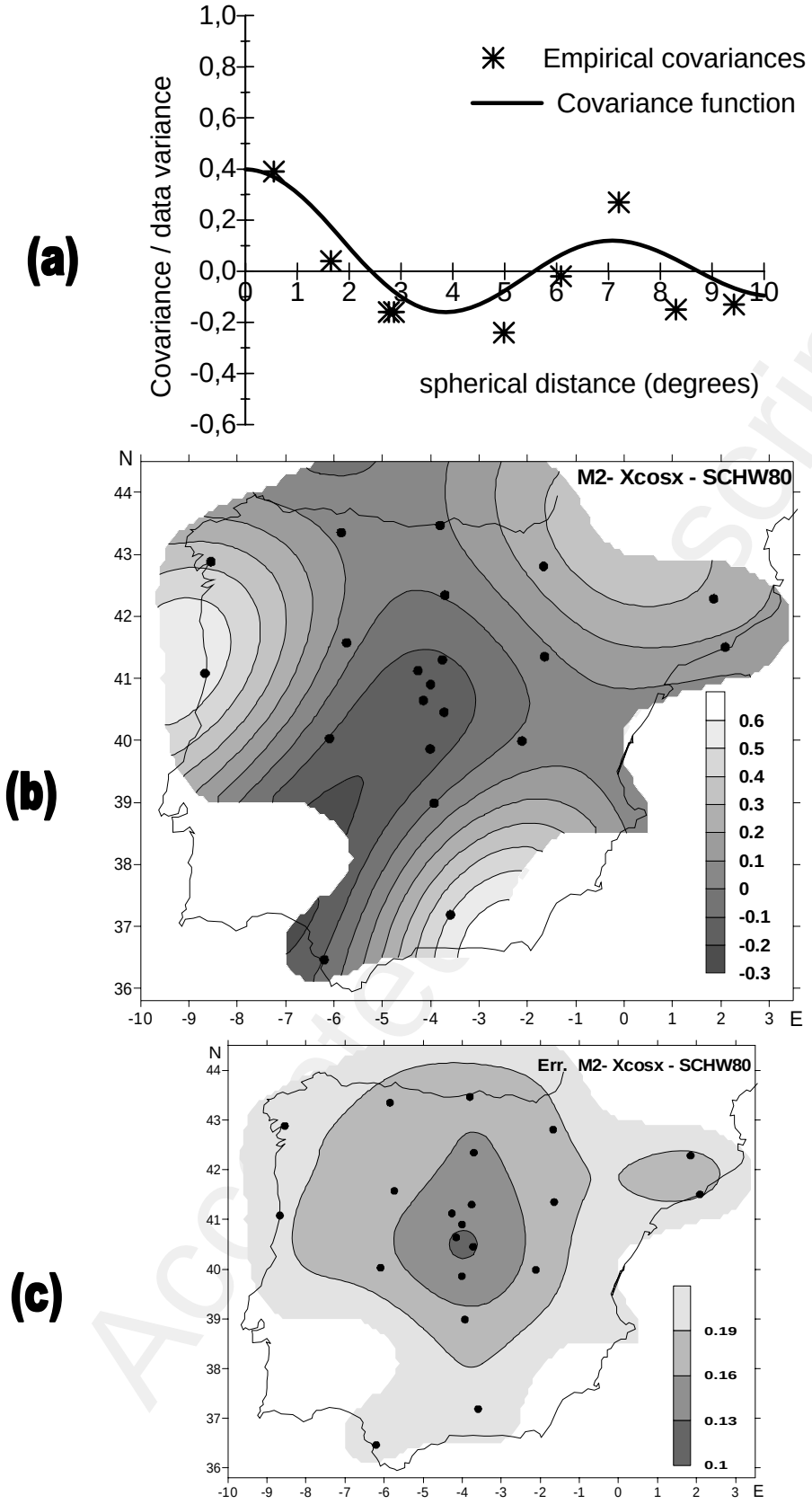


**Figure 3**

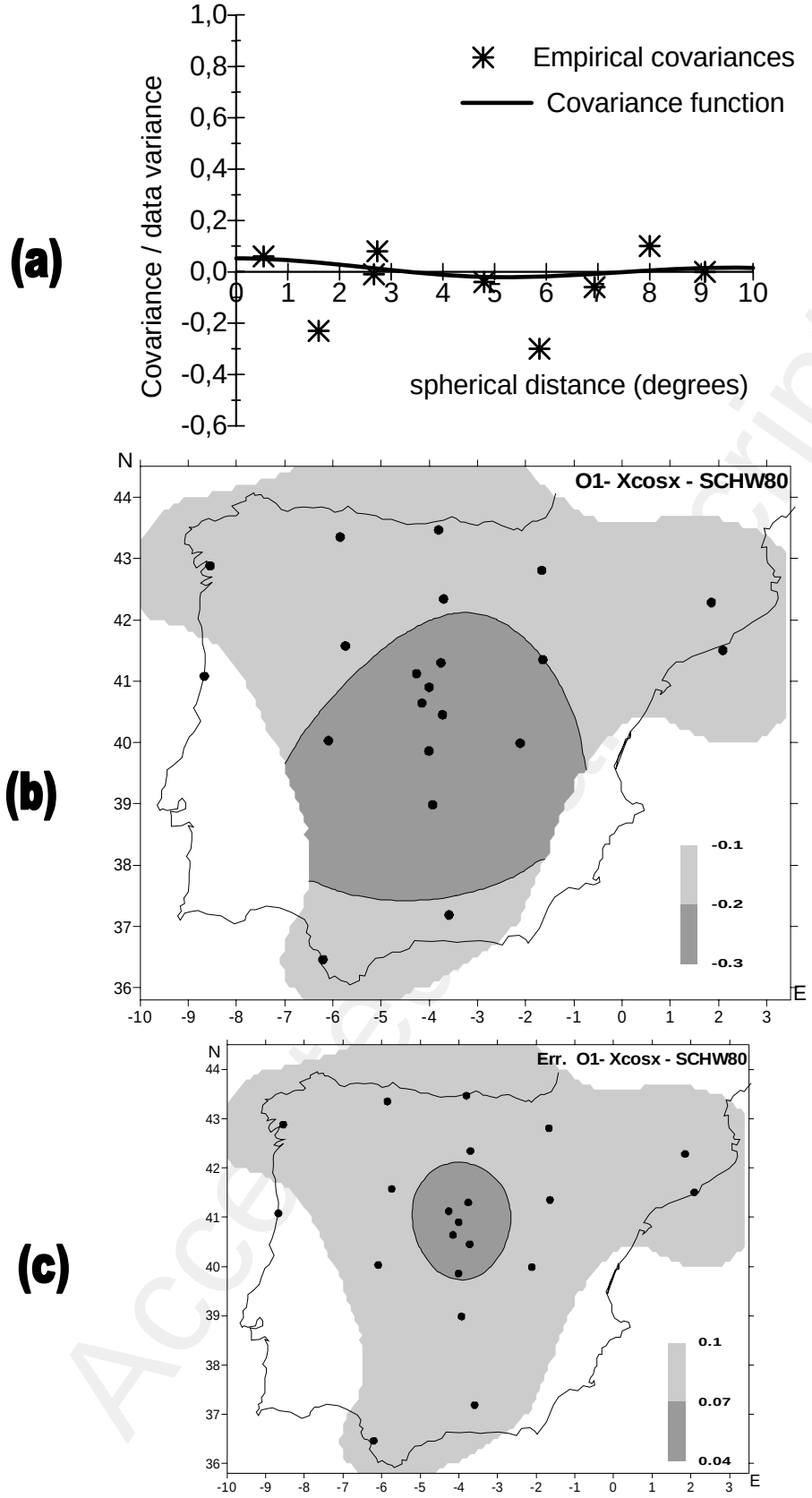


**Figure 4**

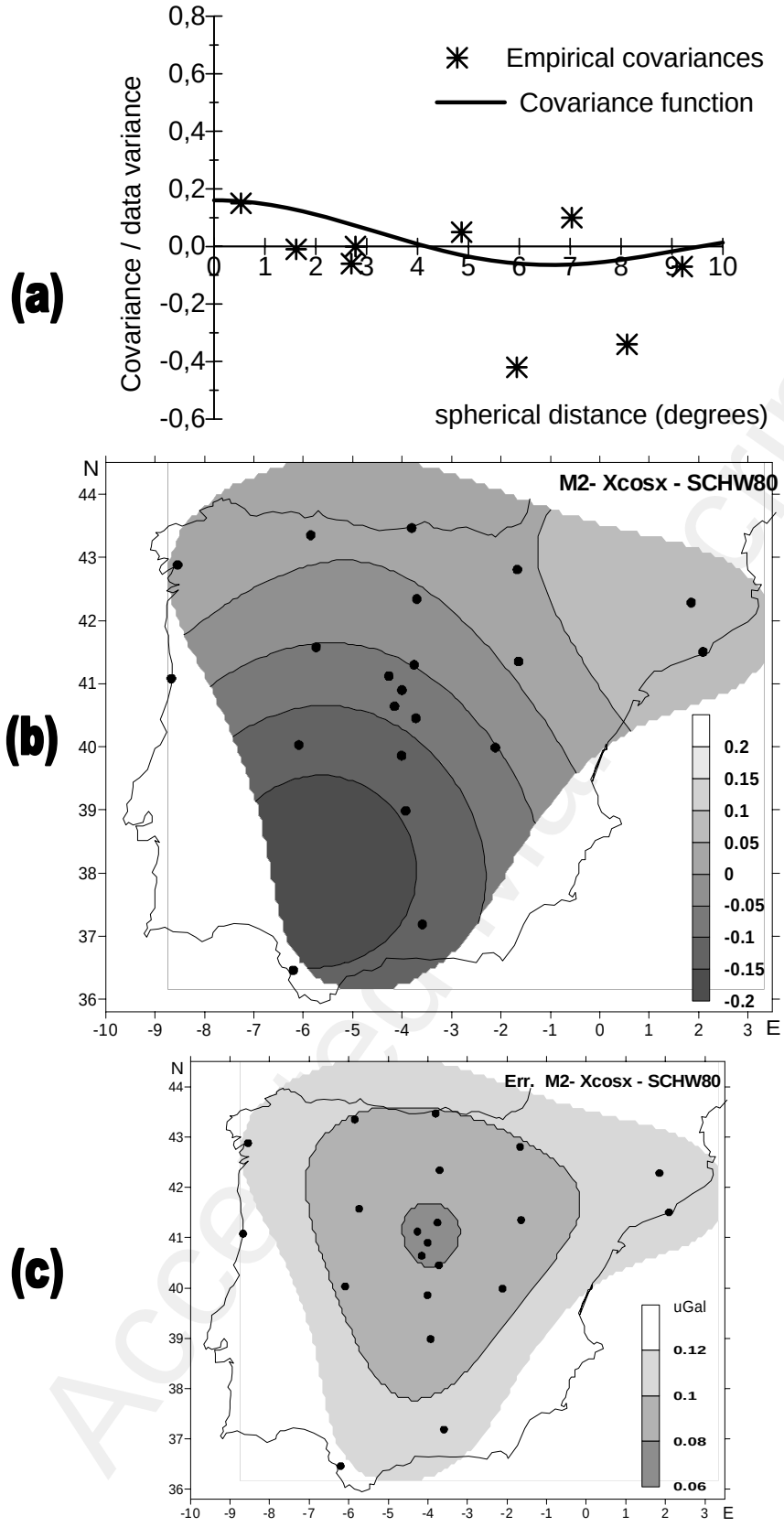


**Figure5**

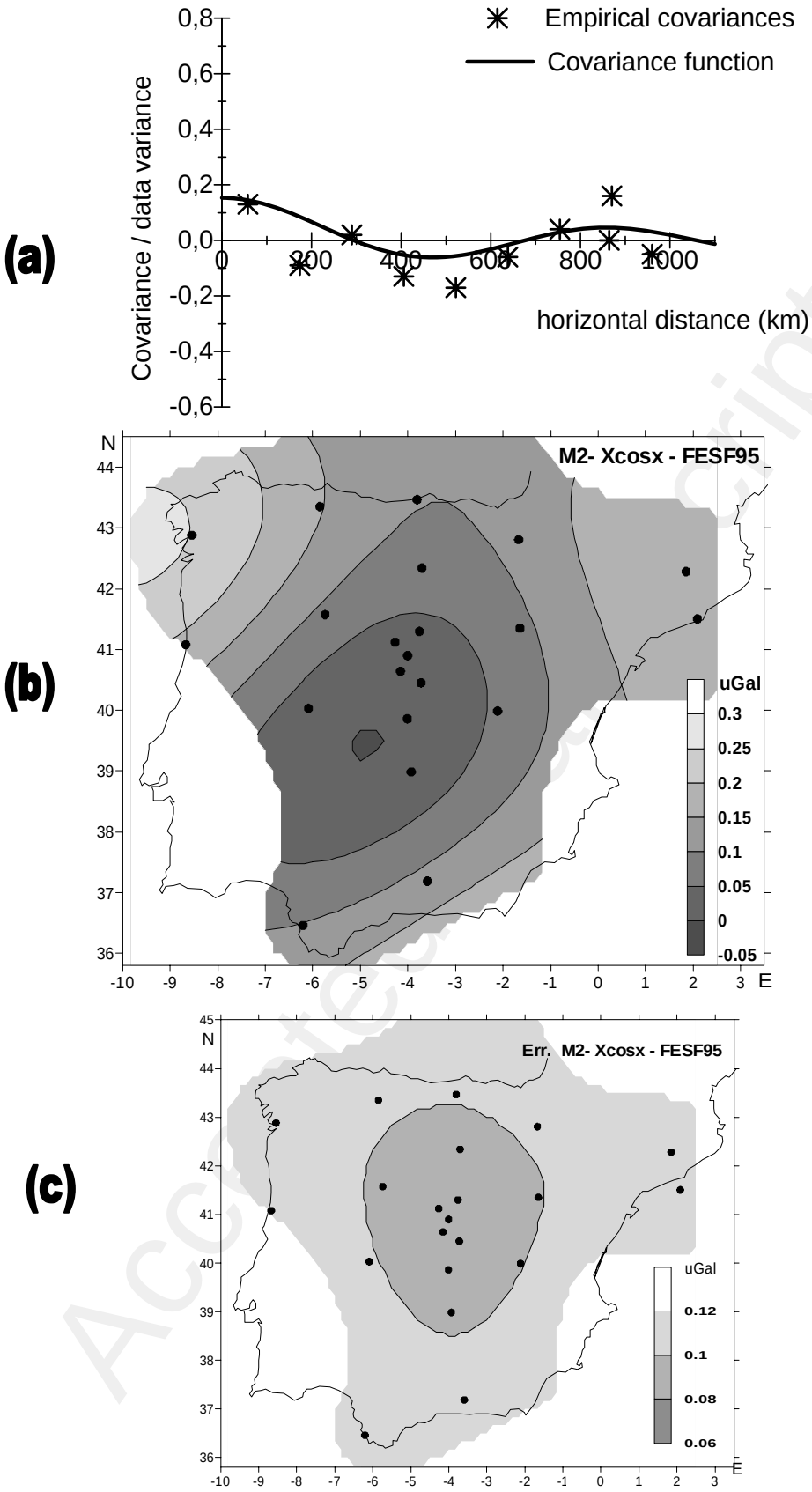


**Figure 6**

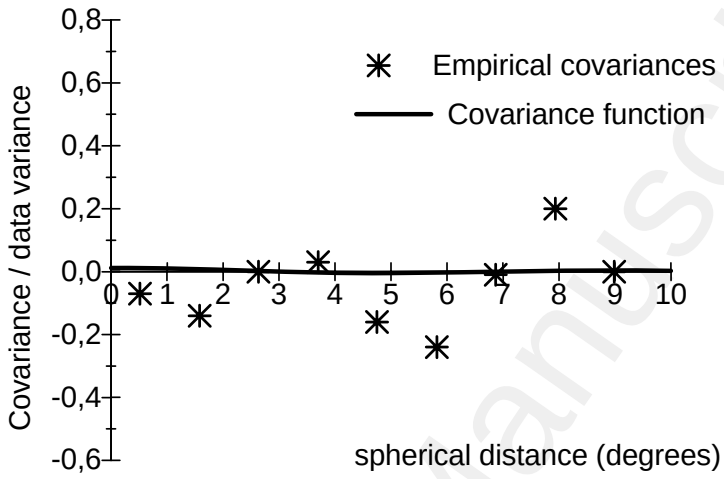


**Figure 7**

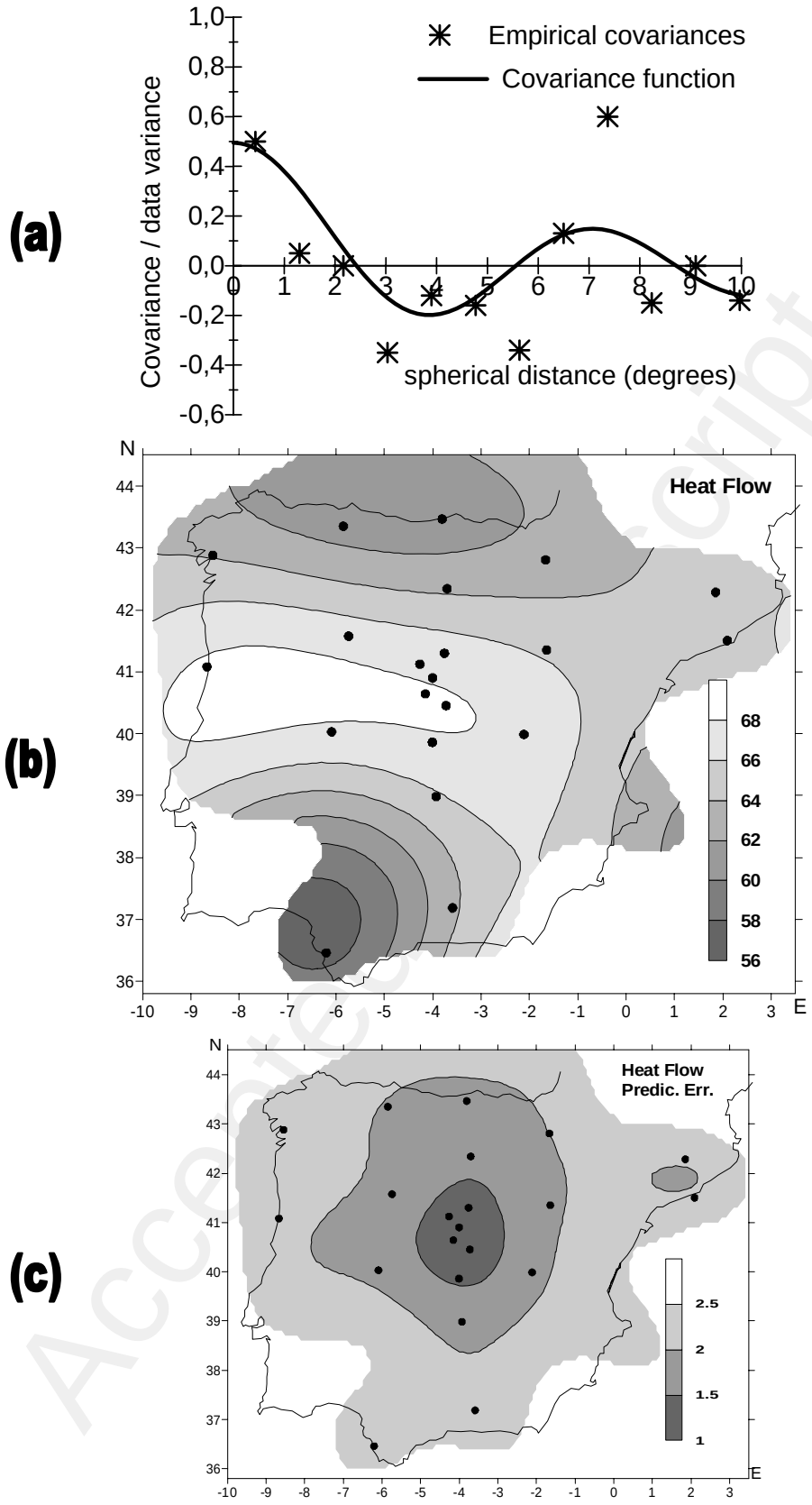


**Figure 8**